Master's Thesis of Engineering

Triangularity effect on the ExB shearing rate in tokamak plasmas

토카막 플라즈마의 ExB 층밀림율에 대한 삼각도의 영향

August 2023

Graduate School of Engineering
Seoul National University
Nuclear Engineering Major

Qingyun Hu

Triangularity effect on the ExB shearing rate in tokamak plasmas

Advisor: Yong-Su Na

Submitting a master's thesis of
Engineering

August 2023

Graduate School of Energy Systems Engineering
Seoul National University
Nuclear Engineering Major

Qingyun Hu

Confirming the master's thesis written by
Qingyun Hu
August 2023

Chair	Taik Soo Hahm	(Seal)
Vice Chair	Yong-Su Na	(Seal)
Examiner	Gyungjin Choi	(Seal)

Abstract

Triangularity effect on the ExB shearing rate in tokamak plasmas

Qingyun Hu

Department of Energy Systems Engineering

The Graduate School

Seoul National University

It has been shown in TCV and DIII-D experiments that negative triangularity (NT) tokamak plasmas could achieve H-mode-level confinement even without the H-mode transition. It is widely accepted that ExB flow shear suppression of turbulence and transport plays a crucial role in confinement improvement and transport barrier formation in fusion plasmas. In this thesis, a study of the triangularity effects on the ExB shearing rate is performed. I employ Miller's magnetic equilibrium model, which contains various shaping effects, including triangularity, elongation, and Shafranov shift. Using Miller's model, I derive an analytic expression of the Hahm-Burrell ExB shearing rate, which explicitly shows the contributions of shaping factors. I discuss the isolated effect of shaping factors on the poloidal variation of the shearing rate in terms of flux-squeezing. Two identical discharges in DIII-D are selected for analyses where the triangularity is the only difference; one is NT and the other is positive

triangularity (PT). Using kinetic EFIT reconstruction data of these discharges, the ExB shearing rates are evaluated by carefully distinguishing the contribution from the triangularity to those from the radial electric field and magnetic shear. Finally, I discuss the highly anisotropic features of the ExB shearing rate.

Keywords: triangularity, shaping effect, ExB flow shear, turbulence, tokamak transport, tokamak confinement

Student Number: 2021-25364

Contents

Chapter 1

Introduction

1.1 NT plasma research in tokamaks

H-mode tokamak scenarios [1] have long been considered as options for fusion reactors. But the Edge-Localized modes (ELMs), especially type-I ELMs in H-mode pedestals, induce significant heat flux on PFCs which is an important issue that remains to be solved. In recent years, much attention has been paid to ELM-free plasma operations, including Quiescent H-mode [2], I-mode [3], and ELM-suppressed or mitigated scenarios [4, 5]. ELM-free scenarios have been developed relying on internal transport barriers rather than the edge transport barrier such as FIRE mode [6]. A change of plasma shape from PT to NT was also found to have H-mode like confinement with an L-mode like edge witout ELMs.

Since 1997, improved confinement has been reported in TCV operations with NT [7, 8]. Higher electron energy confinement time has been

observed in NT plasma compared with its positive counterpart. And it has been reported in recent TCV and DIII-D experiments that NT tokamak plasmas could achieve H-mode-level confinement with $H_{89} \sim 1.2$ even without the H-mode transition [9–11], accompanied by a reduction of turbulence level. In the experiments, the L-H transition power threshold has been observed to be higher than PT cases. Without transitions to H-mode, the challenges from type-I ELMy H-mode could be avoided. The DIII-D experiments have achieved a high normalized beta with $\beta_N \sim 2.5$, which is a good signal for fusion gain if it could be extrapolated to a future reactor. Furthermore, the NT plasma shows a linear relation between heating power and plasma stored energy in a limited power range, exhibiting no confinement degradation [10]. However, the initial ASDEX-U experiment on NT plasms showed H-mode like power degradation [12].

Instabilities in NT plasma have been investigated in many theoretical works. In some parameter regimes, NT exhibits stabilizing effects on TEM and ITG [13–15]. Stabilized micro-instabilities could account for enhanced confinement. On the other hand, it has been pointed out that the MHD stability region is narrowed by NT [16–19]. The predicted β_N limit in NT plasmas is lower than PT, unfavorable for fusion gain [20]. The onset of peeling-ballooning modes limits the formation of pedestals. Research on Kinetic Ballooning mode (KBM) in spherical tokamak parameter regimes also showed a restricted second stability window by NT [21]. The onset of MHD instabilities could degrade the confinement, thus prohibiting the L-H transition.

Recent works have shown that residual zonal flow is significantly reduced by NT [14, 22] and that the peak $E \times B$ flow shear bifurcates with

the sign change of the triangularity, maximal off from the low-field-side (LFS) midplane in NT [23]. These have been suggested as explanations for the higher L-H transition threshold in NT compared with PT plasmas.

1.2 ExB flow shearing theory

Microscale turbulence driven by micro-instabilities induces anomalous transport in tokamaks [24]. Enhanced transport degrades the confinement of particles and energy, prohibiting the plasma from achieving burning conditions. Therefore, understanding and regulating turbulence-driven transport is one of the central topics for realizing burning plasmas. It has been widely accepted that (mean) $E \times B$ flow shear suppression of turbulence and transport plays a crucial role in confinement improvement and transport barrier formation in fusion plasmas [25–30]. H-mode was discovered in the ASDEX Tokamak in the early 1980s [1]. In H-mode, a sheared radial electric (E_r) field develops in the ETB region. The mechanism of $E \times B$ shearing suppression was proposed that the sheared $E \times B$ flow suppresses turbulence by tearing turbulence eddy [31]. When a turbulence eddy is present in a background flow with shear in the transverse direction to the flow direction, the eddy elements are decorrelated. Transport reductions have been observed in plasma operations when the $E \times B$ shearing rate exceeds the turbulence growth rate [25]. The decorrelation theory has been experimentally tested both qualitatively and quantitatively, not only in H-mode but also in Very-High (VH) mode and the formation of core transport barriers, see a comprehensive review in Ref. [30]. In the middle-1980s, the theory was extended, incorporating the effects of magnetic shear, and became applicable for general magnetic

configurations [32–34]. Since the formation of core transport barriers is found to be facilitated by a non-monotonic shear or at least a flat q profile [30, 35–37]. It has been shown in a recent work that the strong edge magnetic shear at the diverted KSTAR plasma facilitates $E \times B$ shear suppression of turbulence and H-mode transition [38]. A more recent simulation work suggests that the magnetic shear induces a positive or negative effect on the flow shearing of turbulence, depending on the competition of the E_r shear and the magnetic shear dependencies of the flow shear [39]. In general axisymmetric toroidal geometry, the shearing rate exhibits in-out asymmetric characteristics [40], resulting in the in-out asymmetry of radial decorrelation of turbulence. Plasma elongation, as one of the most important shaping factors, has been found to enhance the shearing rate [41]. Recently, the theory of $E \times B$ shear suppression has been further extended, considering the initially tilted turbulence eddies routinely observed in nonlinear simulations [42]. The relative sign of the flow shear and initial tilting angle of the eddy has been found to impact the shearing suppression efficiency. In island geometry, theories associated with the anisotropic features of $E \times B$ flow shear have been developed for the vortex flow in magnetic islands [43, 44]. Turbulence can advect across the island due to the deviation of the flow streamline from the magnetic line.

The $E \times B$ flow comes from the $E \times B$ drift velocity, which reads:

$$\vec{u}_E = \frac{\vec{E} \times \vec{B}}{B^2}. \tag{1.1}$$

Conventionally, the (mean) $E \times B$ flow shear refers to the equilibrium component of $E \times B$ flow shear, while the zonal flow shear is the nonlinear component. They both contribute to the suppression of turbulence, but

this thesis focuses on the (mean) $E \times B$ flow shear. The equilibrium radial electric field is measured by the radial force balance of the ions:

$$E_r = \frac{1}{n_{\mathrm{i}} e Z_{\mathrm{i}}} \nabla P_{\mathrm{i}} - u_\theta B_\phi + u_\phi B_\theta. \tag{1.2}$$

Equation (1.2) indicates the dependence of the $E \times B$ flow shear on the pressure gradient, toroidal angular momentum, and poloidal flow. Considering that the flow shear also impacts turbulence and transport, there are several different regimes that with various dependence on E_r and E_r shear, resulting in different feedback loops of flow shear-turbulence-transport. For example, both u_θ and ∇P_i are important in the H-mode edge, u_ϕ is of more importance in VH mode, and both u_ϕ and ∇P_i are thought to be important in core transport barriers [25].

The general $E \times B$ shearing rate in a shaped tokamak plasma, the so-called "Hahm-Burrell formula", is [33]

$$\omega_s = \frac{\Delta\psi_0}{\Delta\zeta} \frac{\partial^2}{\partial\psi^2} \Phi_0. \tag{1.3}$$

The factor $\nabla\psi_0/\nabla\zeta$ is referred to as the form factor. The radial correlation length of an ambient turbulence eddy is measured as $\Delta r = \Delta\psi_0/RB_\theta$, and the binormal correlation length of the eddy is measured as $\Delta l_\perp = RB_\theta \Delta\zeta/B$. An isotropic eddy shape in the perpendicular plane is assumed, that is, $\Delta r \cong \Delta l_\perp$. Then one has the expression of the shearing rate as follows:

$$\omega_s = \frac{(RB_\theta)^2}{B} \frac{\partial^2}{\partial\psi^2} \Phi_0. \tag{1.4}$$

Here, the definitions of notations follow the conventional. The electric

field potential Φ_0 is assumed as a flux function. This formula works well for general axisymmetric tokamak equilibria, incorporating the geometrical effect through the dependence of B_θ, such as the Shafranov shift, elongation, and triangularity. The main content of this thesis will discuss this issue.

For an intuitive introduction, let's consider a simpler case, the high aspect-ratio version of the flow shearing rate [32, 38]:

$$\begin{aligned} \omega^{(0)}_{E\times B} &= \frac{r}{q}\frac{\partial}{\partial r}\left(\frac{qE_r}{rB}\right) \\ &= r\frac{\partial}{\partial r}\left(\frac{E_r}{rB}\right) + \frac{E_r}{rB}\hat{s}. \end{aligned} \tag{1.5}$$

Here, circular-concentric flux surfaces are assumed. One can tell from the first row of Equation (1.5) that E_r, safety factor q, and curvature all contribute to the flow shear. The second row separates the flow shear into two parts. The first one comes from the dependence of E_r shear [31]. The second term comes from the dependence of magnetic shear $\hat{s}$. The equation indicates that the E_r shear and magnetic shear could both result in radial decorrelation of turbulence eddies. E_r shear and magnetic shear could tilt the eddies in co-direction or counter-directions, so they could have positive or negative synergy, depending on the parameter regimes where the plasma locates.

For effective $E \times B$ shearing of turbulence eddies, the shearing rate must be comparable to $\Delta\omega_D$, the nonlinear turbulence decorrelation rate in the absence of $E \times B$ shear [31]. For stabilization of micro-instabilities, the shearing rate must be comparable to γ_{max}, the maximum linear growth rate of the most unstable mode [45, 46].

1.3 Objective and structure of this work

Improved confinement and increased L-H transition power thresholds in NT plasmas have been demonstrated in many tokamak devices [7, 10, 12]. Particulary, NT plasma in DIII-D shows asymmetric wave-number spectra, indicating flow shearing of turbulence [11]. And NT plasma in ASDEX-U exhibits a shallower E_r profile, which links the $E \times B$ flow shear to the higher L-H transition power threshold [12]. Those observations bring a question of how the $E \times B$ flow shearing is impacted by NT. The triangularity effect enters the flow shearing rate through either the form factor or the radial electric field profile. In this work, I study (I) the triangularity effect on the form factor in the L-mode tokamak plasma regime; (II) the triangularity effect on the radial profile of flow shear in DIII-D plasmas with matched triangularity; (III) the triangularity effect on the isotropic feature of the flow shear DIII-D plasmas with matched triangularity.

In Chapter 2, I employ the Miller's equilibrium model for a description of the equilibrium magnetic field structure. It is based on a general axisymmetric toroidal equilibrium. Geometrical factors are considered, including the Shafranov shift, triangularity, and elongation. This equilibrium model could be further extended for higher poloidal Fourier components, such as Squareness. One can parameterize physical quantities like safety factor q, magnetic shear $\hat{s}$ with shaping factors. Thus the shaping factor dependence would be revealed.

In Chapter 3, I transform the Hahm-Burrell shearing rate with respect to the Miller's equilibrium model. To be specific, I choose to express the

poloidal field B_θ and toroidal field B_ϕ in terms of local safety factor ν, curvature radius r_s, and a scale factor $|\nabla r|$. The resulting formula explicitly shows the shaping factor dependence of the shearing rate. And the scale factor $|\nabla r|$ is of primary interest in this thesis because it contains the essential shaping effect and impacts the shearing rate as a whole.

Section 3.1 presents an analysis of the form factor in a simplified way that facilitates interpretation. I narrow down the scope of analysis to a high aspect-ratio configuration. Thus the poloidal variation of the form factor is primarily determined by $|\nabla r|$. I present both intuitive illustrations and mathematical demonstrations of the shaping effect on the variation.

Section 3.2 presents an analysis of the normalized form factor based on the experimental data from DIII-D. I map the MHD equilibria to the Miller's model so as to calculate the normalized form factor with parameters from matched plasma with a mirrored triangularity. I discuss the triangularity effect on the poloidal variation of the form factor and the radial extension of the effect.

Section 3.3 presents an analysis of the radial profile of the shearing rate based on experimental data from DIII-D. I discuss the radial features of the shearing rate in the NT plasma, more specifically, the inward-moving of the radial peak of the shearing rate.

Section 3.4 presents an analysis with combined calculation results in Section 3.2 and Section 3.3. I discuss the highly anisotropic feature of the flow shear and its impact on the anisotropic feature of the transport.

Chapter 2

Miller's local equilibrium model

This chapter presents the study of the triangularity dependence of the $E\times B$ shearing rate in general tokamak geometry [33] that uses the Miller's local equilibrium model. It could accurately parameterize the D-shaped flux surface of tokamak plasmas [47]. Extensions of the Miller D-shape model can be found in Refs. [48–50]. The Miller's model uses the standard formula for the shape of a flux surface given by

$$\begin{aligned} R &= R_0(r) + r\cos\left\{\theta + \left[\sin^{-1}\delta(r)\right]\sin\theta\right\}, \\ Z &= \kappa(r) r \sin\theta. \end{aligned} \tag{2.1}$$

where the minor radius r and the poloidal magnetic flux ψ have a one-to-one relation, i.e., $r = r(\psi)$, $\psi = \psi(r)$, and θ is the poloidal angle. Figure 2.1 shows an example of a D-shaped flux surface. The radial gradient of major radius, $\partial_r R_0$ is referred to as the Shafranov shift gradient [47]. Shaping factors $\delta(r)$ and $\kappa(r)$ denote triangularity and elongation of the flux surface, respectively. I consider an axisymmetric equilibrium mag-

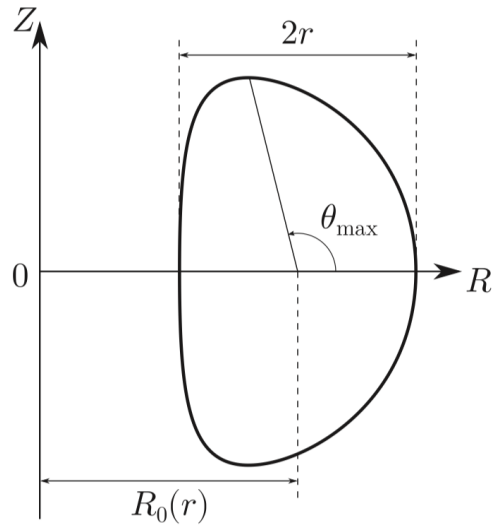

Figure 2.1 Illustration of a flux surface in the Miller's model [51].

netic field $\vec{B} = \nabla\phi \times \nabla\psi + I(\psi)\nabla\phi$ [52]. The poloidal magnetic field reads

$$B_\theta = \frac{|\nabla\psi|}{R} = \frac{d\psi}{dr}\frac{|\nabla r|}{R}, \tag{2.2}$$

and the toroidal magnetic field reads

$$B_\phi = \frac{I}{R}. \tag{2.3}$$

For a direct comparison to previous works [31, 32, 38], it is convenient to work with the local safety factor ν [53], which is written as

$$\nu(\psi,\theta) = \frac{\vec{B}\cdot\nabla\phi}{\vec{B}\cdot\nabla\theta} = \frac{IJ_r}{R^2\partial_r\psi} = \frac{r_s B_\phi}{RB_\theta}. \tag{2.4}$$

where $J_r = (\nabla r \times \nabla\theta \cdot \nabla\phi)^{-1}$ is the Jacobian for the transformation from toroidal coordinates (R, Z, ϕ) to a flux coordinate system (r, θ, ϕ). And

$r_s = dl/d\theta = J_r|\nabla r|/R$ is the radius of curvature [49, 54], where dl denotes a differential length element along the curve in (R,Z) cross-section. It measures the bending of magnetic surfaces, which contains the shaping effects of triangularity δ and elongation κ. In the near-circular concentric tokamaks, one has $r_s \approx r$. It recovers a widely used approximate expression of the safety factor q from equation (2.4). However, in a general tokamak, the two radii r_s and r are different due to shaping effects.

The Jacobian matrix for the transformation from toroidal coordinates (R, Z, ϕ) to a flux coordinate system (r, θ, ϕ) reads [55]

$$\begin{pmatrix} \frac{\partial r}{\partial R} & \frac{\partial r}{\partial Z} & 0 \\ \frac{\partial \theta}{\partial R} & \frac{\partial \theta}{\partial Z} & 0 \\ 0 & 0 & 1 \end{pmatrix} = \begin{pmatrix} \frac{\partial R}{\partial r} & \frac{\partial R}{\partial \theta} & 0 \\ \frac{\partial Z}{\partial r} & \frac{\partial Z}{\partial \theta} & 0 \\ 0 & 0 & 1 \end{pmatrix}^{-1} \tag{2.5}$$

Then the Jacobian is obtained as

$$\begin{aligned} J_r =& (\nabla r \times \nabla \theta \cdot \nabla \phi)^{-1} \\ =& r\kappa R\{[\frac{\partial R_0}{\partial r} + \cos(\theta + x\sin\theta) - s_\delta \sin(\theta + x\sin\theta)\sin\theta]\cos\theta \\ &+ (1 + x\cos\theta)\sin(\theta + x\sin\theta)\sin\theta(s_\kappa + 1)\}, \end{aligned} \tag{2.6}$$

where $x = \sin^{-1}\delta$ is an equivalent of the triangularity δ. Factors $s_\kappa = r\partial_r\kappa/\kappa$ and $s_\delta = r\partial_r\delta/\sqrt{1-\delta^2}$ denote the radial gradients of the elongation κ and the triangularity δ, repsectively.

Chapter 3

Triangularity effects on flow shearing rate

The general $E \times B$ shearing rate for an isotropic turbulent eddy in a shaped tokamak plasma is [33, 38]

$$\omega_s \cong \frac{(RB_\theta)^2}{B_\phi} \frac{\partial^2}{\partial \psi^2} \Phi_0, \tag{1.4}$$

where the electric potential $\Phi_0 = \Phi_0(\psi)$ is a flux function. Note that the form factor $(RB_\theta)^2/B_\phi$ has been known to give shaping effects to the $E \times B$ shearing rate including anisotropy on a flux surface, which results in the in-out asymmetry of the $E \times B$ shearing [27, 33, 40]. The radial electric field E_r is given by

$$E_r = -\frac{\partial \Phi_0}{\partial \psi} RB_\theta. \tag{3.1}$$

Expressing the poloidal field B_θ in terms of ν and r_s and using equation (3.1), one can rewrite equation (1.4) as

$$\omega_s = \frac{r_s}{\nu}\frac{\partial}{\partial r}(\frac{\nu E_r}{r_s B_\phi})|\nabla r|. \tag{3.2}$$

Note that equation (3.2) is a direct generalization of the $E \times B$ shearing rate in Ref. [32] for a high aspect ratio near-circular plasma. The scale factor $|\nabla r|$ in equation (3.2) is a result of the choice of the radius r in the Miller's model which satisfies $d\psi/dr = RB_\theta/|\nabla r|$. It's inverse value measures the distance between flux surface elements on nearby surfaces. Note that a convenient relation $d\psi = RB_\theta dr$ doesn't hold here. The equation could be separated into two parts as follows [38] using the local magnetic shear $s = (r/\nu)d\nu/dr$:

$$\omega_s = \left[r_s \frac{\partial}{\partial r}(\frac{E_r}{r_s B_\phi}) + \frac{E_r}{rB_\phi}s\right]|\nabla r|. \tag{1.5}$$

The first term in equation (1.5) is a direct generalization of the Biglari-Diamond-Terry (BDT) $E \times B$ shearing rate [31] obtained in cylindrical plasma, and the second term gives the magnetic shear contribution [38]. Note that the effect of the radius of curvature r_s enters only in the first term [31] while the scale factor $|\nabla r|$ impacts both terms. The expressions of the two factors can be obtained as follows from equation (2.1).

$$r_s = r\sqrt{(1 + x\cos\theta)^2 \sin^2(\theta + x\sin\theta) + \kappa^2\cos^2\theta}, \tag{3.3}$$

and

$$
\begin{aligned}
|\nabla r| =& \kappa^{-1}[\sin^2(\theta + x\sin\theta)(1 + x\cos\theta)^2 + \kappa^2\cos^2\theta]^{1/2} \\
& \times \{\cos(x\sin\theta) + \partial_r R_0 \cos\theta \\
& + [s_\kappa - s_\delta\cos\theta + (1 + s_\kappa)x\cos\theta]\sin\theta\sin(\theta + x\sin\theta)\}^{-1}.
\end{aligned} \tag{3.4}
$$

Note that in this study, I keep the contributions from the gradients of the (elongation and) triangularity and show that they are as influential as the triangularity itself.

3.1 Shaping factor dependence of the form factor

In the picture of $E \times B$ flow shearing suppression of turbulence, the efficiency of $E \times B$ flow shearing is significantly impacted by the match between the mode structure of turbulence and the poloidal profile of the flow shearing rate. The form factor in the equation (1.4) determines the poloidal variation of the flow shearing rate. Thus, in this section, I study the effect of shaping factors on the flow shearing rate via the form factor. In the Miller's model, one can transform the form factor as follows:

$$
\frac{(RB_\theta)^2}{B} \cong R|\nabla r|^2 \frac{\psi'^2}{I}. \tag{3.5}
$$

One can tell from Equation (3.5) that the poloidal variation of the form factor is determined by factor $R|\nabla r|^2$. For high aspect ratio configurations, the variation of $R(r,\theta)$ is not considered to be significant. In this section, I focus on the factor $|\nabla r|$, which plays a key role in the shaping effect. Figure 3.1 shows a schematic representation of the triangularity effect. Here, the distance between flux surface elements on nearby surfaces could be measured by $\delta r/|\nabla r|$. At different poloidal locations,

triangularity induces poloidally varying distances. Factor $|\nabla r|$ increases when the distance becomes smaller and decreases when the distance becomes larger. As a result, it bifurcates in the low-field-side (LFS) in a PT case but peaks at the high-field-side (HFS) midplane in a NT case. Since the poloidal magnetic field is proportional to $|\nabla r|$ in the relation $B_\theta = |\nabla r|\psi'/R$, the triangularity effect on the form factor could also be interpreted in terms of flux-squeezing. In a region where the field line is more densified, the magnetic field is stronger.

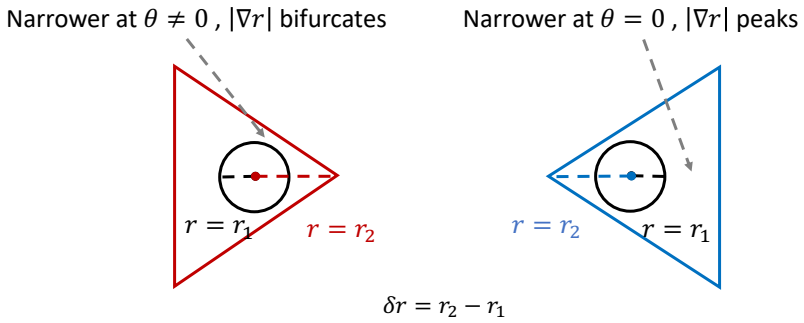

Figure 3.1 Illustration of the isolated effect of triangularity on flux-squeezing. Here, the effect of triangularity is exaggerated.

For a mathematical demonstration of this interpretation, I show the poloidal profile of $|\nabla r|$ with the isolated effect of PT and NT in Figure 3.2 and 3.3, respectively. One can clearly tell the bifurcation of $|\nabla r|$ in the LFS of the PT case and the peak at the LFS midplane of the NT case. Here, the effects of triangularity are exaggerated, which means the effects of the Shafranov shift and elongation are not considered. In realistic cases, the Shafranov shift will weaken the peaks in the HFS of the NT case and, in the meantime, enhance the peak at the LFS midplane.

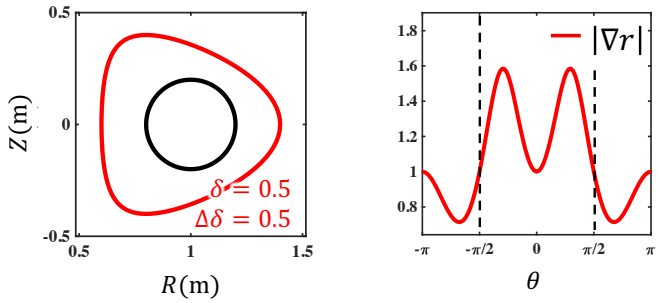

Figure 3.2 Isolated effect of PT on flux-squeezing.

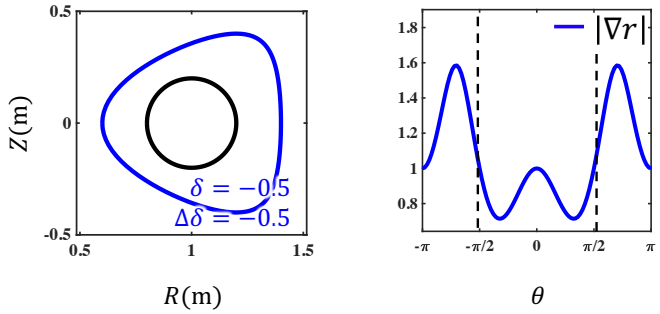

Figure 3.3 Isolated effect of NT on flux-squeezing.

Figure 3.4 illustrates the effect of the Shafranov shift and elongation. In L-mode plasmas, the sign of the Shafranov shift is typically negative. The shift makes the inner surface closer to the outer surface in the $\vec{R}$ direction. In other words, it squeezes the flux at the LFS. So, it tends to enhance the LFS peaks or bifurcations induced by triangularity. However, elongation induces an in-out symmetrical effect on $|\nabla r|$. It could either enhance or reduce the triangularity effects, depending on the sign of κ'.

In addition, factor $|\nabla r|$ could also serve as a "Gradient geometrical factor", connecting the flux coordinate profiles with spatial profiles [7].

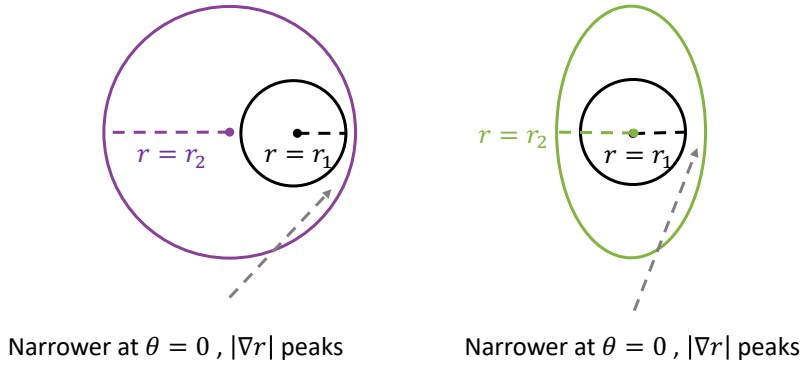

Figure 3.4 Illustration of the isolated effect of Shafranov shift and elongation on flux-squeezing.

For example, if the temperature T is assumed to be a flux function, the gradient of the temperature could be expressed as $|\nabla T| = (dT/dr)|\nabla r|$. Recall the criterion of ITG instability is a critical value of $-R\nabla T_i/T_i$ [56]. Factor $|\nabla r|$ impacts the criterion locally, resulting in impacted local turbulence transport. In shaped toroidal geometry, one can expect that the flow shear and turbulence transport share the same poloidal characteristics to some extent. The up-down symmetry of the modes and the flow shear would be directly related to the symmetry of the factor. Besides, from Fourier's law $\vec{Q} = -k\nabla T$, the local characteristics of diffusivity is also related to ∇r.

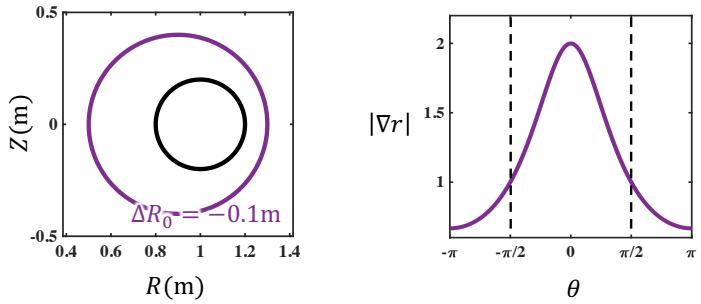

Figure 3.5 Isolated effect of Shafranov shift on flux-squeezing.

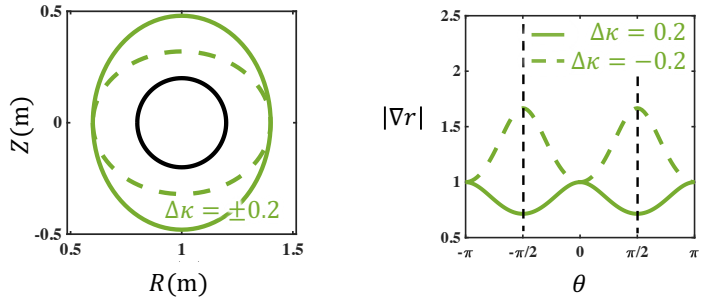

Figure 3.6 Isolated effect of Shafranov shift on flux-squeezing.

3.2 Normalized form factor of PT and NT plasmas

I have addressed the isolated shaping factor dependence of the form factor in Section 3.1 focusing on $|\nabla r|$. Yet, one should note that the parameter dependence of the form factor is complicated in reality. Not to say that the shaping factors have their correlations. Thus, that simple picture may become invalid in some cases. In this section, I study the triangularity effect by looking into experimental equilibria.

I take global MHD equilibria in matched triangularity experiments (DIII-D shots: #170672 and #170680 at t = 1.380s). Their boundary triangularities are mirrored, but I_p and B_T on the axis are the same. From the $\psi(R, Z)$ data of those equilibria, I extract the shapes of flux surfaces. Then I mapped the shapes into the Miller's model and obtained the profiles of shaping factors as functions of radial coordinate ψ_N. At each radial location, the poloidal variation of the form factor is different because of the difference in shaping factors. Figure 3.7 and (3.8) show normalized form factor for those equilibria in the (ψ_N, θ) space. Here, the form factor is normalized in such a way that for each radial location, the poloidal profiles are normalized by their corresponding peak values. One can tell from Figure 3.7 that the form factor or flow shearing rate bifurcates in LFS in PT plasma. In contrast, as shown in Figure 3.8, the flow shearing rate peaks at the LFS midplane.

Moreover, by comparing the profiles at the inner-most radial location, one can tell that the shaping effect on the form factor extends deeply into the core. It could contribute to the impact of triangularity on global con-

finement. Turbulence tends to localize at LFS mid-plane at the edge. However, in the core, turbulence usually shows a broader poloidal distribution. If that still holds true in NT, a decrease in the shearing efficiency could be expected in the core. Another possibility is that the turbulence drive responds strongly to the flux squeezing, as mentioned in Section 3.1. Then, the turbulence mode structure would also peak at the LFS midplane, consistent with the peaks of flow shear. The shearing efficiency would be maintained. To characterize the core distribution of turbulence, gyrokinetic simulations are needed.

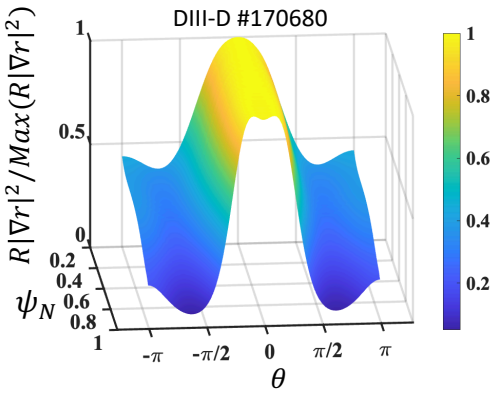

Figure 3.7 Normalized form factor in the (ψ_N, θ) space for the PT case. Parameters are from the MHD equilibrium of DIII-D shot:#170680 at t = 1.380s.

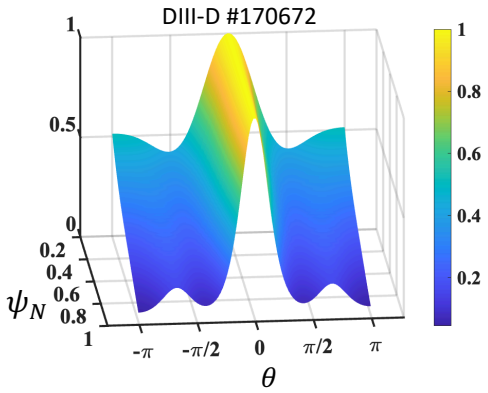

Figure 3.8 Normalized form factor in the (ψ_N, θ) space for the NT case. Parameters are from the MHD equilibrium of DIII-D shot:#170672 at t = 1.380s.

3.3 Radial profiles of the ExB shearing rate in PT and NT plasmas

I have discussed the effect of triangularity on the poloidal variation of the $E \times B$ shearing rate in Section 3.1 and Section 3.2. However, to pursue the interpretation of the triangularity effect on the $E \times B$ shearing rate, the radial variation of the shearing rate is also important. Besides, the amplitude of the shearing rate and its radial profile is also crucial in interpreting the role of the flow shear in the confinement and L-H transition. In this section, I will discuss the radial profiles of the $E \times B$ shearing rate.

As one can tell in Equation (1.4), the amplitude of the shearing rate is modulized by factor $\partial^2\Phi_0/\partial\psi^2$. Considering the profile of E_r in the DIII-D plasma, I calculated the $E \times B$ shearing rate at the LFS midplane, i.e., $\theta = 0$. Figure 3.9 shows the profiles of the shearing rate. Note that the radial coordinate is the square root of the normalized toroidal flux. The PT plasma exhibits strong flow shear at the edge. In contrast, the NT plasma exhibits a peak of flow shear in the core region. The enhancement of flow shear in NT plasma spans a large radial range. Without loss of shearing efficiency, it would result in more significant turbulence suppression in the core. Interestingly, the NT case shows a peak near $\rho = 0.9$, more inward than where the pedestal top often locates in DIII-D H-modes. This peak of the $E \times B$ shearing rate can not only suppress turbulence locally but also inhibit turbulence from spreading inward and inhibits turbulence transport from spreading outward [57–60]. As a result, the core fluctuation would be reduced, and flue deposition gets facilitated.

Better core condition compared to PT L-mode plasma could be expected. On the other hand, turbulence coming from strong resistive turbulence and scrape-off layer turbulence dominates the edge. The formation of edge transport barriers is relatively more difficult with weaker flow shear, which could result in a higher L-H transition power threshold. In addition, it has been reported in a recent BOUT++ simulation work that the peak of $E \times B$ flow shear moves inward in NT H-mode plasmas, compared to PT H-mode plasmas [61]. That indicates the inward moving of the flow shear is generic for NT plasmas regardless of L or H modes and may intrinsically come from the feature of the magnetic field structure. Specifically, stronger flux squeezing at the LFS midplane results in a more significantly peaked poloidal field.

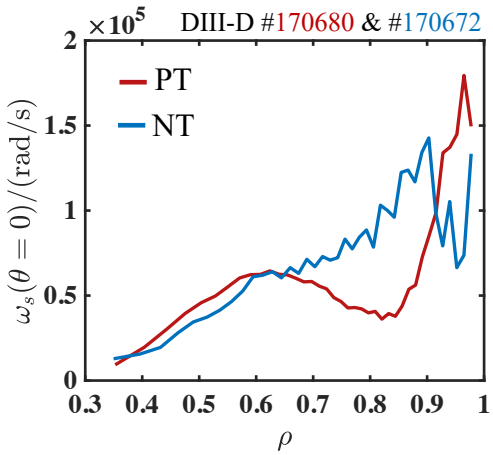

Figure 3.9 Radial profiles of the $E \times B$ shearing rate at LFS midplane. Here, the radial coordinate ρ is the square root of normalized toroidal flux. Parameters are from the same DIII-D equilibrium in Figure 3.7 and 3.8. The corresponding radial electric field data are considered here.

Recall the dependence of the flow shear on the E_r shear and magnetic shear mentioned in Chapter 1.2. Here I discuss the dependencies in the NT plasma. Equation (1.5) explicitly shows the dependence of the flow shear on the local magnetic shear $s = (r/\nu)d\nu/dr$. Figure 3.10 shows the radial profiles of the Hahm-Burrell shearing rate ω_s, the BDT shearing rate ω^{BDT}, and the magnetic shear contribution term, all at $\theta = 0$. Figure 3.10 (a) and (b) are for the PT and NT plasma cases, respectively.

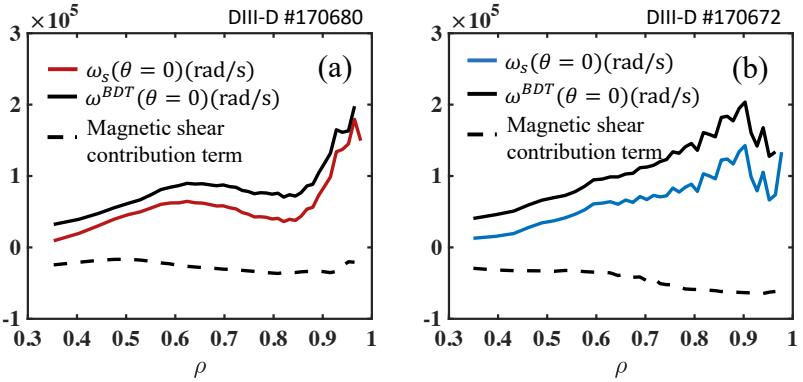

Figure 3.10 Contribution of magnetic shear to ω_s in (a) PT and (b) NT plasma. Parameters are from the same DIII-D data as in Figure 3.9.

The two terms in Equation (1.5) are written as

$$\omega^{BDT} = r_s \frac{\partial}{\partial r}\left(\frac{E_r}{r_s B_\phi}\right)|\nabla r|, \tag{3.6}$$

and

$$\omega_s - \omega^{BDT} = \frac{E_r}{r B_\phi} s|\nabla r|. \tag{3.7}$$

The relative sign of them is mainly determined by the gradient of the radial electric field $\partial_r E_r$, the radial electric field E_r, and the local magnetic shear s. A positive synergistic effect would be expected when

$\partial_r E_r$ and $E_r s$ have the same sign. Two examples of it would be: (i) $\partial_r E_r \cdot E_r < 0$ and $s > 0$, which is possible for H-mode pedestals [38]; (ii) $\partial_r E_r \cdot E_r < 0$ and $s < 0$, which is possible for reversed shear.

However, the DIII-D equilibrium data of both the PT and NT plasmas shows that negative E_r approaches 0 from $\rho = 0.6$ to $\rho = 1$. And the plasmas have monotonically increasing q profiles. That means, at the edge, $\partial_r E_r \cdot E_r < 0$ and $s > 0$, which explains the negative contributions from the magnetic shear. Note that NT plasmas in ASDEX-U exhibit zero-crossing of the E_r profile near the edge. Thus, a positive contribution from magnetic shear is expected at the edge [12]. The dashed lines in Figure 3.10 (a) and (b) indicate a stronger magnetic shear dependence of the flow shear in NT plasma. The enhancement comes from a larger $|E_r|$ and a stronger flux squeezing which enters via $|\nabla r|$.

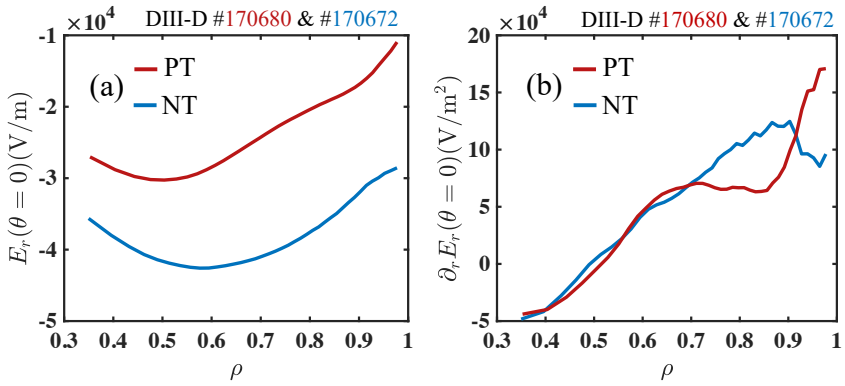

Figure 3.11 Radial profile of (a) E_r and (b) $\partial_r E_r$ at the LFS midplane in the PT and the NT plasma. Parameters are from the same DIII-D data as in Figure 3.9.

In fact, the radial electric field E_r also depends on the magnetic field

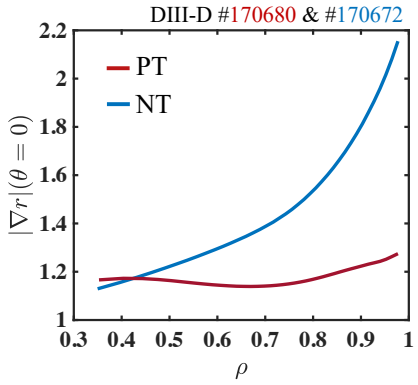

Figure 3.12 Radial profile of $|\nabla r|$ at the LFS midplane in the PT and the NT plasma. Parameters are from the same DIII-D data as in Figure 3.9.

structure. Equation (1.2), the radial force balance equation of ions could be transformed as:

$$E_r = \frac{\nabla r}{n_{\rm i} e Z_{\rm i}} \frac{\partial}{\partial r} P_{\rm i} - u_\theta B_\phi + u_\phi B_\theta. \tag{1.2}$$

The effect of flux squeezing enters the first term via $\nabla P_{\rm i} = \nabla r \frac{\partial}{\partial r} P_{\rm i}$. The enhanced flux squeezing in the NT plasma could make the dependence of E_r on the ion pressure gradient $\nabla P_{\rm i}$ more pronounced. Thus, the ion pressure gradient limited by peeling-ballooning modes [16–18] would limit E_r at the edge. But in the core region, $\rho < 0.9$, the larger $|\nabla r|$ would enhance E_r and E_r shear. Figure 3.11 shows that at $\rho = 0.9$, factor $|\nabla r|$ in NT increases by a factor of roughly 1.5 compared to PT. The increase results in the enhanced ω^{BDT} through both $\partial_r E_r$ and $|\nabla r|$ itself.

The flow shear layer with a peaked flow shearing rate could be regarded as a transport barrier. As the plasma triangularity becomes more negative, the flux-squeezing effect could get further enhanced. The radial

peak of the flow shear would move farther inward. Hence, the transport barrier (or flow shear layer) moves farther inward, allowing edge and scrape-off layer turbulence to spread in until touching the barrier. In the meantime, the edge ion pressure would be further limited by peeling-ballooning modes, inhibiting the formation of edge transport barriers. On the other hand, with auxiliary heating power increased, the internal transport barrier would move outward [12]. With sufficient heating power, the edge transport barriers would come into being. Here, the outward moving induced by enhanced heating could originate from the competition between the three terms in Equation (1.2). A careful look into the evolution of kinetic profiles is needed.

3.4 Anisotropic features of the ExB shearing rate in PT and NT plasmas

Provided that tokamak transport has been known to exhibit anisotropic features, the study is motivated to discuss the isotropic features of the flow shear.

Figure 3.13 and 3.14 shows the $E \times B$ shearing rate in (r, θ) space. As I have shown in Figure 3.7 and 3.9, the flow shearing rate in the PT plasma bifurcates and has large amplitudes at the edge. This indicates that a bifurcation of flow shear does not have to be accompanied by a reduction of its amplitude. In the case of bifurcated strong flow shear, the tolerance of the ballooning angle shift could be improved than the peaked flow shear. As a result, shearing suppression of turbulence would be enhanced, and pedestal formation could be facilitated. For the NT plasma, as I have shown in Figure 3.8 and 3.9, the flow shearing rate peaks at the LFS midplane and exhibits larger amplitude in the core.

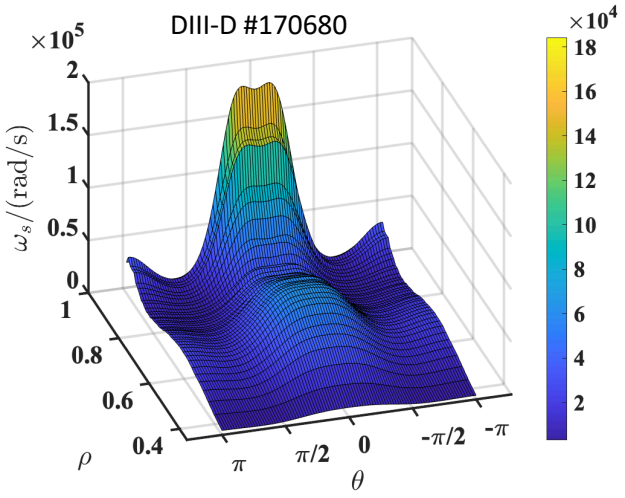

Figure 3.13 $E \times B$ shearing rate in the (ρ, θ) space for the PT case. Parameters are from the same DIII-D data as in Figure 3.9.

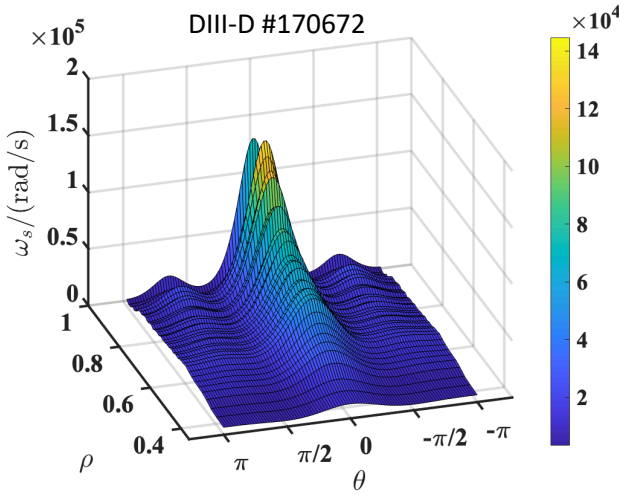

Figure 3.14 $E \times B$ shearing rate in the (ρ, θ) space for the NT case. Parameters are from the same DIII-D data as in Figure 3.9.

Chapter 4

Conclusions

In this thesis, I derived an analytical expression of the Hahm-Burrell ExB flow shearing rate using the Miller's model. Based on this expression, I studied the triangularity effect on the form factor, radial profile, and anisotropic features of the ExB shearing rate. Adopting the data from DIII-D experiments with mirrored triangularity, I found that the flow shear bifurcates in LFS in PT plasma but peaks at the LFS midplane in NT plasma. Also, the radial profile of the flow shear in those plasmas exhibited different characteristics. The midplane profile of flow shear in NT plasma peaks in the inner region of the plasma. The flow shear layer in the core could suppress the turbulence locally and inhibit the inward spreading of the turbulence in the outward region. My analysis of this inward-moving of the flow shear layer links the inward-moving with the magnetic squeezing. That is, enhanced flux squeezing induces stronger E_r shear, and they synergize to increase the flow shear in the core. More-

over, the magnetic shear contribution is more significant in NT plasma. Comparing the anisotropic features of the shearing rate in PT and NT plasma, the bifurcated strong flow shear (at the edge) in PT could facilitate the L-H transition. The peaked strong flow shear (in the core) could have higher shearing efficiency that leads to reduced fluctuation.

Bibliography

[1] Fritz Wagner, G Becker, K Behringer, D Campbell, A Eberhagen, W Engelhardt, G Fussmann, O Gehre, J Gernhardt, G v Gierke, et al. Regime of improved confinement and high beta in neutral-beam-heated divertor discharges of the ASDEX tokamak. *Physical Review Letters*, 49(19):1408, 1982.

[2] KH Burrell, ME Austin, DP Brennan, JC DeBoo, EJ Doyle, C Fenzi, C Fuchs, P Gohil, CM Greenfield, RJ Groebner, et al. Quiescent double barrier high-confinement mode plasmas in the DIII-D tokamak. *Physics of Plasmas*, 8(5):2153–2162, 2001.

[3] DG Whyte, AE Hubbard, JW Hughes, B Lipschultz, JE Rice, ES Marmar, M Greenwald, I Cziegler, A Dominguez, T Golfinopoulos, et al. I-mode: an H-mode energy confinement regime with L-mode particle transport in Alcator C-Mod. *Nuclear Fusion*, 50(10):105005, 2010.

[4] TE Evans, RA Moyer, JG Watkins, PR Thomas, TH Osborne, JA Boedo, ME Fenstermacher, KH Finken, RJ Groebner, M Groth, et al. Suppression of large edge localized modes in high confinement

DIII-D plasmas with a stochastic magnetic boundary. *Journal of nuclear materials*, 337:691–696, 2005.

[5] Jong-Kyu Park, YoungMu Jeon, Yongkyoon In, Joon-Wook Ahn, Raffi Nazikian, Gunyoung Park, Jaehyun Kim, HyungHo Lee, WonHa Ko, Hyun-Seok Kim, et al. 3D field phase-space control in tokamak plasmas. *Nature Physics*, 14(12):1223–1228, 2018.

[6] H Han, SJ Park, C Sung, J Kang, YH Lee, J Chung, TS Hahm, B Kim, J-K Park, JG Bak, et al. A sustained high-temperature fusion plasma regime facilitated by fast ions. *Nature*, 609(7926):269–275, 2022.

[7] J-M Moret, S Franke, H Weisen, M Anton, R Behn, BP Duval, F Hofmann, B Joye, Y Martin, Ch Nieswand, et al. Influence of plasma shape on transport in the TCV tokamak. *Physical review letters*, 79(11):2057, 1997.

[8] Alessandro Marinoni, O Sauter, and S Coda. A brief history of negative triangularity tokamak plasmas. *Reviews of Modern Plasma Physics*, 5(1):6, 2021.

[9] Y Camenen, A Pochelon, R Behn, A Bottino, A Bortolon, S Coda, A Karpushov, O Sauter, G Zhuang, et al. Impact of plasma triangularity and collisionality on electron heat transport in TCV L-mode plasmas. *Nuclear fusion*, 47(7):510, 2007.

[10] Max E Austin, A Marinoni, ML Walker, MW Brookman, JS Degrassie, AW Hyatt, GR McKee, CC Petty, TL Rhodes, SP Smith, et al. Achievement of reactor-relevant performance in negative tri-

angularity shape in the DIII-D tokamak. *Physical Review Letters*, 122(11):115001, 2019.

[11] A Marinoni, ME Austin, AW Hyatt, ML Walker, J Candy, C Chrystal, CJ Lasnier, GR McKee, T Odstrčil, CC Petty, et al. H-mode grade confinement in L-mode edge plasmas at negative triangularity on DIII-D. *Physics of Plasmas*, 26(4):042515, 2019.

[12] T Happel, T Pütterich, D Told, M Dunne, R Fischer, J Hobirk, RM McDermott, U Plank, et al. Overview of initial negative triangularity plasma studies on the ASDEX Upgrade tokamak. *Nuclear Fusion*, 63(1):016002, 2022.

[13] Alessandro Marinoni, Stephan Brunner, Y Camenen, S Coda, JP Graves, X Lapillonne, A Pochelon, O Sauter, and L Villard. The effect of plasma triangularity on turbulent transport: modeling TCV experiments by linear and non-linear gyrokinetic simulations. *Plasma Physics and Controlled Fusion*, 51(5):055016, 2009.

[14] JM Duff, BJ Faber, CC Hegna, MJ Pueschel, and PW Terry. Effect of triangularity on ion-temperature-gradient-driven turbulence. *Physics of Plasmas*, 29(1):012303, 2022.

[15] Gabriele Merlo and Frank Jenko. Interplay between magnetic shear and triangularity in ion temperature gradient and trapped electron mode dominated plasmas. *Journal of Plasma Physics*, 89(1):905890104, 2023.

[16] A Merle, O Sauter, and S Yu Medvedev. Pedestal properties of H-modes with negative triangularity using the EPED-CH model. *Plasma Physics and Controlled Fusion*, 59(10):104001, 2017.

[17] Samuli Saarelma, Max E Austin, M Knolker, Alessandro Marinoni, Carlos Paz-Soldan, Lothar Schmitz, and Philip B Snyder. Ballooning instability preventing the H-mode access in plasmas with negative triangularity shape on the DIII–D tokamak. *Plasma Physics and Controlled Fusion*, 63(10):105006, 2021.

[18] AO Nelson, C Paz-Soldan, and S Saarelma. Prospects for H-mode inhibition in negative triangularity tokamak reactor plasmas. *Nuclear Fusion*, 62(9):096020, 2022.

[19] Junhyuk Song, Carlos Paz-Soldan, and Jungpyo Lee. Impact of negative triangularity plasma shaping on the n= 0 resistive wall mode in a tokamak. *Nuclear Fusion*, 61(9):096033, 2021.

[20] Jacob A Schwartz, Andrew Oakleigh Nelson, and Egemen Kolemen. To dee or not to dee: costs and benefits of altering the triangularity of a steady-state DEMO-like reactor. *Nuclear Fusion*, 62(7):076006, 2022.

[21] Robert Davies, David Dickinson, and H Wilson. Kinetic ballooning modes as a constraint on plasma triangularity in commercial spherical tokamaks. *Plasma Physics and Controlled Fusion*, 64(10):105001, 2022.

[22] Rameswar Singh and PH Diamond. Zonal flow screening in negative triangularity tokamaks. *Nuclear Fusion*, 62(12):126073, 2022.

[23] Rameswar Singh and PH Diamond. A closer look at mean $E \times B$ shearing rate in negative triangularity tokamaks. Submitted to Nuclear Fusion, 2023.

[24] EJ Doyle, WA Houlberg, Y Kamada, V Mukhovatov, TH Osborne, A Polevoi, G Bateman, JW Connor, JG Cordey, T Fujita, et al. Plasma confinement and transport. *Nuclear Fusion*, 47(6):S18, 2007.

[25] KH Burrell. Effects of E × B velocity shear and magnetic shear on turbulence and transport in magnetic confinement devices. *Physics of Plasmas*, 4(5):1499–1518, 1997.

[26] PW Terry. Suppression of turbulence and transport by sheared flow. *Reviews of Modern Physics*, 72(1):109, 2000.

[27] TS Hahm. Physics behind transport barrier theory and simulations. *Plasma physics and controlled fusion*, 44(5A):A87, 2002.

[28] Fritz Wagner. A quarter-century of H-mode studies. *Plasma Physics and Controlled Fusion*, 49(12B):B1, 2007.

[29] L Schmitz. The role of turbulence–flow interactions in L-to H-mode transition dynamics: recent progress. *Nuclear Fusion*, 57(2):025003, 2017.

[30] KH Burrell. Role of sheared E × B flow in self-organized, improved confinement states in magnetized plasmas. *Physics of Plasmas*, 27(6), 2020.

[31] Hamed Biglari, PH Diamond, and PW Terry. Influence of sheared poloidal rotation on edge turbulence. *Physics of Fluids B: Plasma Physics*, 2(1):1–4, 1990.

[32] Taik Soo Hahm. Rotation shear induced fluctuation decorrelation in a toroidal plasma. *Physics of plasmas*, 1(9):2940–2944, 1994.

[33] TS Hahm and KH Burrell. Flow shear induced fluctuation suppression in finite aspect ratio shaped tokamak plasma. *Physics of Plasmas*, 2(5):1648–1651, 1995.

[34] Taik Soo Hahm. E × B shearing rate in quasisymmetric plasmas. *Physics of Plasmas*, 4(11):4074–4078, 1997.

[35] RC Wolf. Internal transport barriers in tokamak plasmas. *Plasma Physics and Controlled Fusion*, 45(1):R1, 2002.

[36] JW Connor, T Fukuda, X Garbet, C Gormezano, V Mukhovatov, M Wakatani, et al. A review of internal transport barrier physics for steady-state operation of tokamaks. *Nuclear Fusion*, 44(4):R1, 2004.

[37] Katsumi Ida and Takaaki Fujita. Internal transport barrier in tokamak and helical plasmas. *Plasma Physics and Controlled Fusion*, 60(3):033001, 2018.

[38] TS Hahm, DH Na, JW Lee, JW Park, YS Na, SS Kim, WH Ko, PH Diamond, Hogun Jhang, and YM Jeon. E × B shear suppression of turbulence in diverted H-mode plasmas: role of edge magnetic shear. *Nuclear Fusion*, 53(9):093005, 2013.

[39] YC Chen, YQ Qin, GY Sun, and Z Lin. The performance of equilibrium radial electric field shear on microturbulence with different magnetic shears in tokamak plasmas. *Plasma Physics and Controlled Fusion*, 65(7):075005, 2023.

[40] YW Cho, Sumin Yi, JM Kwon, and TS Hahm. In-out asymmetry of zonal flow shear and turbulence reduction. *Physics of Plasmas*, 23(10):102312, 2016.

[41] Lei Qi, Jae-Min Kwon, TS Hahm, Sumin Yi, and MJ Choi. Characteristics of trapped electron transport, zonal flow staircase, turbulence fluctuation spectra in elongated tokamak plasmas. *Nuclear Fusion*, 59(2):026013, 2019.

[42] GJ Choi and TS Hahm. E × B shear effect on initially tilted tokamak turbulence eddies. *Nuclear Fusion*, 55(9):093026, 2015.

[43] TS Hahm, YJ Kim, PH Diamond, and GJ Choi. Anisotropic E × B shearing rate in a magnetic island. *Physics of Plasmas*, 28(2), 2021.

[44] GJ Choi and TS Hahm. Long Term Vortex Flow Evolution around a Magnetic Island in Tokamaks. *Physical Review Letters*, 128(22):225001, 2022.

[45] RE Waltz, RL Dewar, and X Garbet. Theory and simulation of rotational shear stabilization of turbulence. *Physics of Plasmas*, 5(5):1784–1792, 1998.

[46] JE Kinsey, RE Waltz, and J Candy. The effect of plasma shaping on turbulent transport and E × B shear quenching in nonlinear gyrokinetic simulations. *Physics of Plasmas*, 14(10), 2007.

[47] RL Miller, MS Chu, JM Greene, YR Lin-Liu, and RE Waltz. Noncircular, finite aspect ratio, local equilibrium model. *Physics of Plasmas*, 5(4):973–978, 1998.

[48] AD Turnbull, YR Lin-Liu, RL Miller, TS Taylor, and TN Todd. Improved magnetohydrodynamic stability through optimization of higher order moments in cross-section shape of tokamaks. *Physics of Plasmas*, 6(4):1113–1116, 1999.

[49] J Candy. A unified method for operator evaluation in local Grad–Shafranov plasma equilibria. *Plasma Physics and Controlled Fusion*, 51(10):105009, 2009.

[50] Ryan Arbon, Jeff Candy, and Emily A Belli. Rapidly-convergent flux-surface shape parameterization. *Plasma Physics and Controlled Fusion*, 63(1):012001, 2020.

[51] O Beeke, M Barnes, M Romanelli, M Nakata, and M Yoshida. Impact of shaping on microstability in high-performance tokamak plasmas. *Nuclear Fusion*, 61(6):066020, 2021.

[52] William D D'haeseleer, William NG Hitchon, James D Callen, and J Leon Shohet. *Flux coordinates and magnetic field structure: a guide to a fundamental tool of plasma theory*, page 174. Springer Science & Business Media, 2012.

[53] John William Connor, RJ Hastie, and John Bryan Taylor. High mode number stability of an axisymmetric toroidal plasma. *Proceedings of the Royal Society of London. A. Mathematical and Physical Sciences*, 365(1720):1–17, 1979.

[54] Thomas F Banchoff and Stephen T Lovett. *Differential geometry of curves and surfaces*, page 18. AK Peters/CRC Press, 2010.

[55] Roscoe B White. *Theory Of Toroidally Confined Plasmas, The*. World Scientific Publishing Company, 2013.

[56] X Garbet, P Mantica, C Angioni, E Asp, Y Baranov, C Bourdelle, R Budny, F Crisanti, G Cordey, L Garzotti, et al. Physics

of transport in tokamaks. *Plasma Physics and Controlled Fusion*, 46(12B):B557, 2004.

[57] WX Wang, TS Hahm, WW Lee, G Rewoldt, J Manickam, and WM Tang. Nonlocal properties of gyrokinetic turbulence and the role of E $\times$ B flow shear. *Physics of plasmas*, 14(7), 2007.

[58] ZH Wang, Patrick H Diamond, Özgür D Gürcan, X Garbet, and XG Wang. Turbulence propagation in heat flux-driven plasmas: implications for temperature profile structure. *Nuclear Fusion*, 51(7):073009, 2011.

[59] Rameswar Singh and Patrick H Diamond. When does turbulence spreading matter? *Physics of Plasmas*, 27(4), 2020.

[60] TS Hahm and PH Diamond. Mesoscopic transport events and the breakdown of Fick's law for turbulent fluxes. *Journal of the Korean Physical Society*, 73:747–792, 2018.

[61] Chenchen Qin, Maolin Mou, Shaoyong Chen, Yongjian Li, Yang Luo, Limin Zhu, Liangkang Dong, and Changjian Tang. Effect of negative triangularity on peeling-ballooning instability. *Physica Scripta*, 98(4):045601, 2023.

Abstract

It has been shown in TCV and DIII-D experiments that negative triangularity (NT) tokamak plasmas could achieve H-mode-level confinement even without the H-mode transition. It is widely accepted that ExB flow shear suppression of turbulence and transport plays a crucial role in confinement improvement and transport barrier formation in fusion plasmas. In this thesis, a study of the triangularity effects on the ExB shearing rate is performed. I employ Miller's magnetic equilibrium model, which contains various shaping effects, including triangularity, elongation, and Shafranov shift. Using Miller's model, I derive an analytic expression of the Hahm-Burrell ExB shearing rate, which explicitly shows the contributions of shaping factors. I discuss the isolated effect of shaping factors on the poloidal variation of the shearing rate in terms of flux-squeezing. Two identical discharges in DIII-D are selected for analyses where the triangularity is the only difference; one is NT and the other is positive triangularity (PT). Using kinetic EFIT reconstruction data of these discharges, the ExB shearing rates are evaluated by carefully distinguishing the contribution from the triangularity to those from the radial electric field and magnetic shear. Finally, I discuss the highly anisotropic features of the ExB shearing rate.

Keywords: triangularity, shaping effect, ExB flow shear, turbulence, tokamak transport, tokamak confinement

Student Number: 2021-25364